Morphological study of P3HT:PCBM blend films prepared through solvent annealing for solar cell applications

Fang-Chung Chen [a,b,*], Chu-Jung Ko [a,c], Jyh-Lih Wu [a,c], Wei-Chi Chen [a,b]

[a] Department of Photonics, National Chiao Tung University, Hsinchu 30010, Taiwan
[b] Display Institute, National Chiao Tung University, Hsinchu 30010, Taiwan
[c] Institute of Electro-optical Engineering, National Chiao Tung University, Hsinchu 30013, Taiwan

A B S T R A C T

We have systematically investigated the morphology of poly(3-hexylthiophene; P3HT) and [6,6]-phenyl C_{61}-butyic acid methyl ester (PCBM) blend films prepared through a slow growth apparoch as a function of PCBM loading in the blends for bulk heterojunction solar cells. In addition to the electrical characterisitcs, the molecular ordering and crystallinity of the polymers was examined by using the UV–vis spectroscopy and grazing incidence X-ray diffraction. From the images of confocal laser scan microscopy, we were also able to *in-situ* monitor the phase separation of the P3HT:PCBM blends during the process of solvent evaporation. Finally, the conductive atomic force microscopy was utilized to probe the spatial distribution of the local current across the photoactive layer prepared with various P3HT:PCBM ratios. From the experimental results, we found that the distribution of PCBM molecules in the P3HT matrix became homogeneous after the solvent annealing process, even though the distribution of the PCBM molecules was not even in the beginning. Therefore, the higher device efficiency could be attributed to the better thin-film morphology of the polymer blends.

1. Introduction

Among the carbon-neutral energy sources, solar cells have been considered as the largest and most promising technology. Besides inorganic photovoltaic devices, solution-proccessed polymer solar cells have spurred much interest because of their advantages of low cost, flexibility, and light weight [1–6]. Further, low-cost fabrication methods, such as full roll-to-roll processes, have also been demonstrated [7–10]. So far, many practical applications, including grid connected polymer solar panels and lamps driven by polymer solar cells, have been presented [11–13]. At present, a power conversion efficiency (PCE) around 4–5% could be routinely fabricated based on a concept called bulk-heterojunction junction (BHJ) [6]. The typical active layer of the BHJ solar cells is composed of one electron-donating polymer, such as poly(3-hexylthiophene; P3HT), and one electron-withdrawing fullerene derivative, such as [6,6]-phenyl C_{61}-butyic acid methyl ester (PCBM). The large amount of the interfaces between these two components in the polymer blends insures that high concentrations of free charge carriers can be generated upon the sun illumination because the chemical potential across the junction helps to overcome the high exction binding energy. More recently, PCE as high as 8.13% has been announced [14].

One of the key issues for achieving a high-efficiency device is the controlling of morphology of the active layer in the polymer solar cells [1–5]. The nanoscale phase separation between the two compounds significantly affects the efficiency of exciton separation as well as the charge transport in the blended films. Many process parameters for the preparation of the active layer, such as the solvent system used to dissolve the polymer blends [15–18] and the annealing temperature during the processes [1,19–22], have been reported as important factors affecting the morphology. Therefore, many approaches, such as thermal annealing [19–22] and solvent annealing [2,23], have been proposed to optimize the thin film morphology.

Different from the thermal treatment, the solvent annealing method attempts to slow down the solvent evaporation rate during the preparation of the active layer. Li et al. [2] were the first to apply a slow growth method for preparing P3HT:PCBM blends in a solvent-saturated environment. To study the improved mechanism, several studies extracted the diode parameters to understand the carrier behavior in the blends. For example, Mihailetchi et al. [24] found that the hole mobility was improved by 33 times. Shrotriya et al. [25] also showed that the efficiency improvement was due to the enhancement of exciton generation rate and dissociation probability.

Although the morphology analysis of P3HT:PCBM thin films has been widely reported, most of the blending thin films were

* Corresponding author at: Department of Photonics, National Chiao Tung University, Hsinchu 30010, Taiwan. Tel.: +886 3 5131484; fax: +886 3 5735601.
E-mail address: fcchen@mail.nctu.edu.tw (F.-C. Chen).

prepared through thermal annealing [19–22,26]. On the other hand, relevant studies on the morphological characteristics and revolutions of the P3HT:PCBM blends during the solvent annealing processes are much less [23–25]. In this work, we systematically investigated the device characterisitcs and the morphology of the photoactive layers prepared through the slow growth apparoch as a function of PCBM loading in the P3HT films. In addition to the electrical characterisitcs, the molecular ordering and crystallinity of the polymers were examined using the UV–vis spectroscopy and grazing incidence X-ray diffraction (GIXRD). Further, from the images of confocal laser scan microscopy (CLSM), we were able to in-situ monitor the phase separation of the P3HT:PCBM blends during the process of solvent evaporation. Finally, the conductive atomic force microscopy (C-AFM) was then utilized to probe the spatial distribution of the local current across the photoactive layer prepared with various P3HT:PCBM ratios. From the results of the study, we found that the two different treatment approaches, namely, solvent and thermal annealing methods, led to different morphologies. Further, we could correlate the device characteristics and the resulting morphology after solvent annealing.

2. Experimental

The polymer solar cells were fabricated on indium tin oxide (ITO)-coated glass substrates. The glass substrates were cleaned sequentially with a detergent, dionized water, acetone, and isopropanol. Afterwards, the substrates were dried in an oven. Prior to the deposition of organic thin films, the ITO substrates were treated with UV-ozone treatment for 15 min. Poly(3,4-ethylenedioxythiophene):poly(styrenesulfonate) (PEDOT:PSS) was then spin-coated onto the substrates and baked at 140 °C for 1 h. The active layer, consisting of P3HT (Rieke Met. Inc.) and PCBM (Nano-C) dissolved in 1,2-dichlorobenzene (DCB), was spin-coated on top of PEDOT:PSS layer. The wet film was then transferred to a Petri dish and subjected to solvent annealing [2]. After the annealing process, the device was further baked at 110 °C for 5 min. Finally, the cathode, comprising of Ca (30 nm) and Al (100 nm), was deposited through a shadow mask. The electrical properties of the solar cells were measured using a Keithley 2400 source-measure unit. The photocurrent was obtained under illumination from a Thermal Oriel solar simulator (AM1.5G). The illumination intensity was calibrated using a standard Si photodiode detector equipped with a KG-5 filter (Hamamatsu Inc.). The calibration method, based on the IEC-69094-1 spectrum, followed the procedures described previously [27]. GIXRD measurements were performed using a Philps X'Pert Pro diffractometer. The incident angle was fixed at $0.3°$ for obtaining the maximum scattering intensity. A monochromatic Cu k_α beam with a wavelength of $\lambda = 0.154$ nm was used as the radiation source. Confocal images were collected with a Leica TCS-SP5 inverted confocal microscope at room temperature. An Argon-ion laser operating at 488 nm was served as the excitation light source. No photobleaching was observed under these conditions after the measurements. The C-AFM measurement was carried in the dark under air ambient conditions. The Au-coated Si tips, with a radius of ca. 20–30 nm, were used for this measurement. The current images were recorded by applying a negative bias on the Si tip at 2.5 V.

3. Results and discussion

Fig. 1(a) shows the current density–voltage (J–V) characteristics under illumination (100 mWcm^{-1}, AM 1.5 G) of the solvent-annealed devices prepared with different P3HT:PCBM weight ratios. From the figure, we could see that the composition ratio strongly influences the

device electrical properties. When the weight ratio of P3HT:PCBM composition was equal to 1:1, the device exhibited the highest power conversion efficiency (3.66%). The values of short-circuit current density (J_{sc}) and fill factor (FF) were 9.53 mAcm^{-2} and 64%, respectively. On the other hand, the open-circuit voltage (V_{oc}) remained unchanged (0.60 V) while the composition varied. Table 1 summarizes the characteristics of the devices in this study. The results were very similar to the that of the previous reports [23,28,29]. For example, Chirvase et al. [28] found that the photocurrent and efficiency showed a maximum while the weight ratio of P3HT:PCBM was between 1:1 and 1:0.9. From the time-of-flight measurement, Huang and Yang [29] suggested that hole and electron mobilities are balanced at this composition.
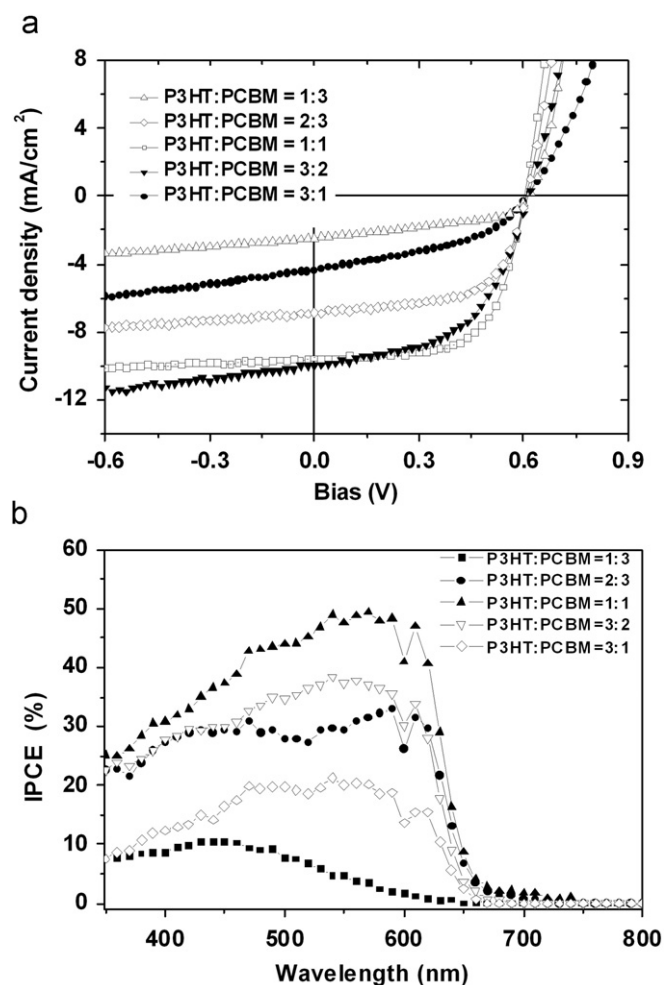

Fig. 1. (a) The J–V characteristics, recorded under 100 mW cm^{-2} illumination (AM 1.5G), of the polymer solar cells prepared with different P3HT:PCBM weight ratios. (b) The corresponding IPCE curves.

Table 1
Photovoltaic characteristics of polymer photovoltaic devices prepared with various P3HT:PCBM compositions.

Ratio of P3HT:PCBM	V_{oc} (V)	J_{sc} (mA/cm^2)	FF (%)	PCE [%]
1:3	0.60	2.48	45.1	0.67
2:3	0.60	6.87	60.7	2.50
1:1	0.60	9.53	64.0	3.66
3:2	0.60	10.10	53.1	3.22
3:1	0.60	4.33	42.8	1.11

Fig. 1(b) shows the corresponding incident photon-to-electron conversion efficiency (IPCE) results of the devices prepared with different compositions. The trends in IPCE follow the of the values of J_{sc}. The best efficiency was obtained at a 1:1 weight ratio blend. Further, the spectra shapes also significantly change while different weight ratios of P3HT:PCBM were used. When the ratio was 1:3, the IPCE spectra has a maximum peak at around 400–500 nm. In the longer wavelength regime, especially within the wavelength range of 500–650 nm; however, the efficiency increased with the increasing composition of P3HT. The shapes of the IPCE spectra were similar to those of the absorption spectra of the polymer blends as showed in Fig. 2. The result indicates that the P3HT molecules have higher ability to absorb photons. However, when the PCBM loading was over 50%, the IPCE was gradually reduced and even the absorption was increased; the result suggested that a possible problem occurred in extracting the charge carriers from the device.

We have shown thus far that the composition ratio of P3HT and PCBM influence significantly on the electrical properties of the photovoltaic devices. To explore such effect, we further utilized the UV–vis and X-ray diffraction spectra to analyze the thin film morphology. Fig. 2 shows the absorption spectra of the P3HT:PCBM films with different compositions. Obviously, the intensity of the UV–vis absorption peaks increased with the P3HT concentrations, suggesting that the main absorption came from P3HT molecules. Further, when the P3HT:PCBM ratio was 3:1, we could clearly observe the three vibronic shoulders, indicating strong interchain-interlayer interactions among the regioregular P3HT chains and high ordering of the polymer chains in the composition films [2]. However, the vibronic peaks gradually disappeared with the increasing PCBM concentrations, suggesting that the interaction of P3HT polymer chains was disrupted by PCBM molecules [30]. The result is consistence with the electrical properties (Fig. 1). The reduced interaction of the P3HT would lower the hole mobility, thereby decreasing the efficiency of the OPVs, especially for the samples in which the PCBM concentration was over 50%.

To further confirm the degree of the ordering, the crystallineity of the P3HT:PCBM composition films was examined using in-plane grazing incidence X-ray diffraction (GIXRD). As shown in Fig. 3, the X-ray diffraction spectra display two sets of reflections, which can be attributed to the reflections of P3HT. The three low-angle diffraction peaks indexed (h 0 0) (h=1–3) are associated with the crystallographic direction along the alkyl side chains (a axis). On the other hand, the peak indexed (0 1 0) is associated with the π-stacking direction of the backbones consisting of polythiophene (b axis) [1]. From the changes of the relative intensities of the (1 0 0) peak
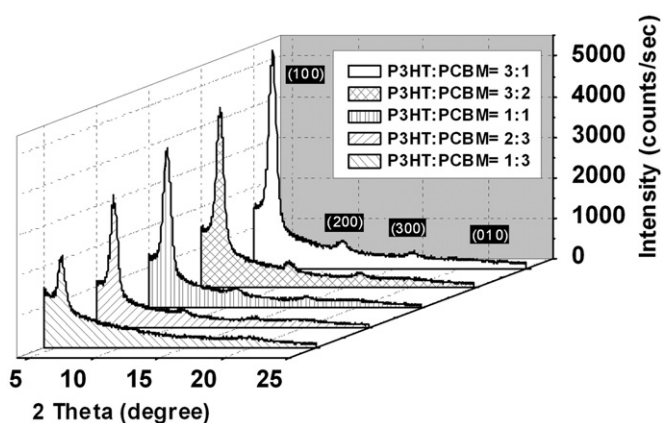

Fig. 3. GIXRD spectra of the polymer blends prepared with different composition ratios. The film thickness of the samples was ~200 nm.
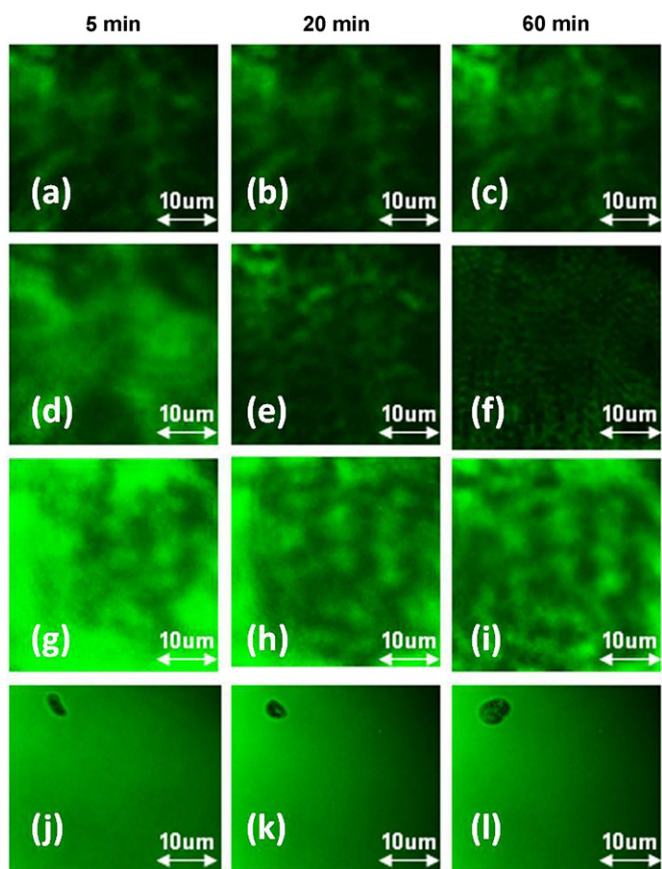

Fig. 4. Time-revolution CLSM images of the polymer blends during the solvent annealing process. The P3HT:PCBM weight ratios are (a)–(c) 1:3; (d)–(f) 1:1; (g)–(i) 3:2; and (j)–(l) 3:1.

($2\theta=5.4°$), we can see that the crystallinity was decreased with increasing PCBM concentration. The result XRD spectra further support the crystallinity revolution as we deduced from the absorption spectra.

To directly probe the revolution of the phase separation in the polymer blends with different composition ratios, we recorded the CLSM images to *in-situ* observe the morphology changes during the solvent annealing process. The confocal microscopy has been used to inspect the phase separation in the polymer blends [30,31]. Fig. 4 shows the fluorescence images of the polymer blends prepared with different composition ratios. The
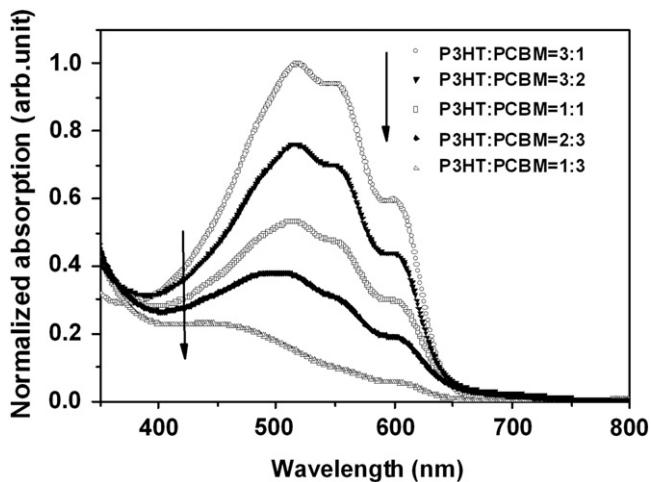

Fig. 2. Absorption spectra of the polymer blends prepared with different composition ratios. The film thickness of the samples was ~200 nm.

bright and dark regimes were assigned as the P3HT-rich and PCBM-rich phases, respectively [30]. In the first 5 min, we can see that the area of the dark regimes increased with the increase in PCBM concentration (Fig. 4(a) (d), (g) and (j)). When the weight ratio of PCBM was down to 25% (P3HT:PCBM=3:1), the PCBM phase was surrounded by the P3HT polymers, where the particle size was around 4 μm long and 2 μm wide (Fig. 4(j)). In addition, we also found that the PCBM particles grew gradually (Fig. 4(j)–(l)). When PCBM concentration further increased, the PCBM grains appeared randomly in the blends. More interestingly, while the PCBM content was 50% (P3HT:PCBM=1:1), the PCBM molecules were dispersed randomly in the first 5 min (Fig. 4(d)); the two phases graduately became a well-ordered structure (Fig. 4(f)), resulting in an ideal morphology, which is close to the so-called "interpentrating network" [32]. However, when the composition ratio deviated from 1:1, we can clearly observed that the distribution of the PCBM-rich domain was not uniform (Fig. 4(i)). The less interfacial area between the P3HT and PCBM molecules probably led to fewer number of excitons generated upon light illumination and the discontinuous conducting pathways may also result in more severly charge trapping in the polymer blend. Finally, when the PCBM loading was increased up to 75%, we can see that the morphology of the polymer blend almost unchanged during the solvent annealing process.

In order to directly correlate the nanoscale phase separation and electrical behavior, we employed the C-AFM to image the local photocurrent distribution in the blends [33]. The conducting probe used was coated with Au, which has a high work function. The sample configuration was ITO/PEDOT:PSS/P3HT:PCBM (Fig. 5(a)); in such samples, the high electron injection barrier between the Au-coated Si tip and the polymer blend blocked the electron injection and only allowed holes transport solely in the p-channel polymer molecules predominately, contributing to the hole-only current. Therefore, we inferred that the bright and

dark regions were corresponding to the P3HT-rich and PCBM-rich domains, respectively. The hole current images for the samples prepared with different composition ratios are shown in Fig. 5(b)–(e). In the sample with 75% PCBM, the current obtained throughout the film was quite small, indicating that hole conduction was not effcient becasue of the limited amount of p-channel material (P3HT; Fig. 5(b)). Further, the distribution of photocurrent was not uniform. While the PCBM concentration was decreased to 50%, the sample exhibited the most homogeneous photocurrent distribution among the different composition conditions (Fig. 5(c)). For the 3:2 P3HT:PCBM film, we can clearly observe two domains (Fig. 5(d)). Note that the dimensions of the phase-separated domains in Fig. 4(f) and Fig. 5(d) are very similar, suggesting that a consistence result was obtained by using these two different probing tools. When the PCBM concentration was further decreased to 25%, a much higher current could be obtained, suggesting a higher hole mobility in the thin film (Fig. 5(d)). This is probably due to the higher level of alignment of P3HT chains. Becasue PCBM molecules would interrupt the self-organization of P3HT polymers, the low PCBM concentration ensured the higher level of alignment. In short, we can see that the current distributions were consistence with the morphological results revealed from the CLSM meansurements (Fig. 4).

Finally, we further compared the surface morphology of the P3HT:PCBM blends prepared either by thermal or solvent annealing approaches. Fig. 6 displays the CLSM image of the P3HT:PCBM thin film after thermal annealing treatment. After thermal annealing at 150 °C for 30 min, an entire different morphology was observed. PCBM molecules were segregated from the blend and crystallized to form a needle-like structure. The PCBM needles were averagely ~8 μm long and randomly dispersed in the P3HT matrix. Similar results were reported by Swinnen et al. [30]. Furthermore, we also found that some of PCBM needles have bright centers, which may be owing to the fact that P3HT existed as the cores in the needle centers after the phase separation.

For solvent annealing treatments, the longer drying time allowed the polymer blend to become a more thermodynamically
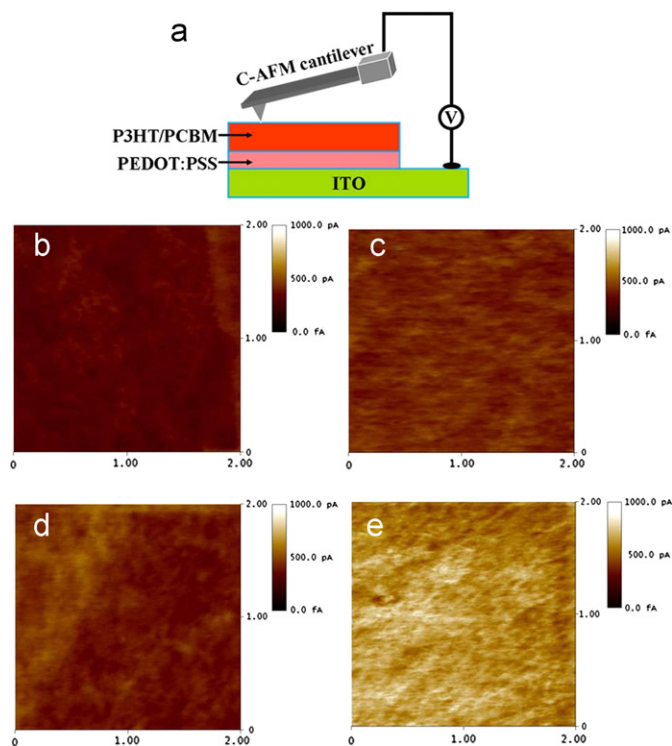

Fig. 5. (a) Schematic representation of the C-AFM experimental setup. (b)–(e) The C-AFM current images of the polymer blends prepared with different P3HT/PCBM ratios. They correspond to the samples prepared with P3HT/PCBM ratios of 1:3; 1:1; 3:2, and 3:1.
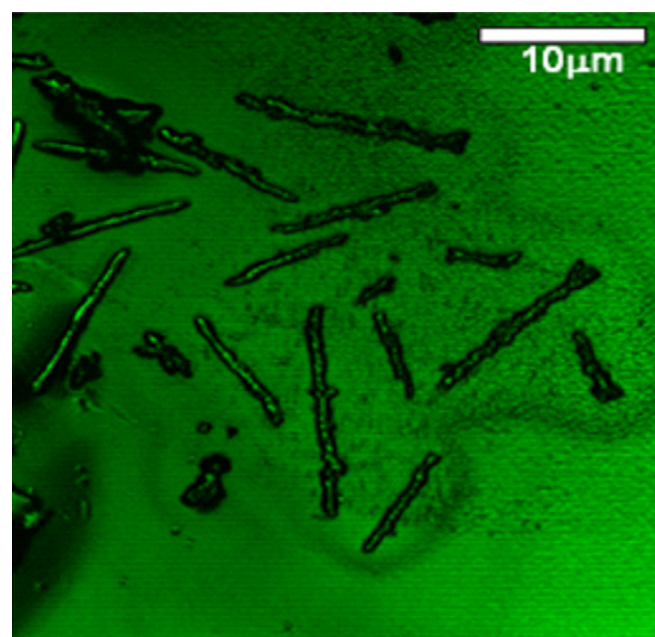

Fig. 6. The CLSM image of the polymer blends prepared through thermal annealing at 150 °C for 30 min. The P3HT:PCBM weight ratio was 1:1.

stable morphology at room temperature. On the other hand, during the thermal annealing, because PCBM molecules probably have a higher mobility at the higher temperature, the nucleation process became more efficient. As a result, we could see larger/longer PCBM needle-like crystals in the P3HT matrix. Therefore, the apparent differences in the film morphology of the polymer films indicated different mechanisms of the phase separation existing for the thin films prepared by either thermal or solvent annealing.

4. Conclusion

In conclusion, we have systematically investigated the effect of the PCBM loading on the device characteristics as well as the morphology of the P3HT:PCBM composite thin films prepared through solvent annealing. At the optimized concentration condition, we in-situ observed that an "interpenetrating-like" morphology was formed during the solvent evaporation process through the CLSM experiments. Even the distribution of PCBM molecules were not even in the beginning, the resulting thin film morphology became homogeneous after the solvent annealing process. Therefore, the higher device efficiency could be attributed to the better thin film morphology of the polymer blends. Finally, the C-AFM directly mapped the p-channel photocurrent throughout the polymer films. The consistance results of CLSM and C-AFM measurements confirmed that the electrical properties indeed highly correlate to the morphology of the photoactive films.

Acknowledgement

References

[1] W.L. Ma, C.Y. Yang, X. Gong, K. Lee, A.J. Heeger, Thermally stable, efficient polymer solar cells with nanoscale control of the interpenetrating network morphology, Adv. Funct. Mater. 15 (2005) 1617–1622.
[2] G. Li, V. Shrotriya, J.S. Huang, Y. Yao, T. Moriarty, K. Emery, Y. Yang, High-performance solution processable polymer photovoltaic cells by self-organization of polymer blends, Nat. Mater. 4 (2005) 864–868.
[3] F.C. Krebs, Fabrication and processing of polymer solar cells: a review of printing and coating techniques, Sol. Energy Mater. Sol. Cells 93 (2009) 394–412.
[4] L.M. Chen, Z. Hong, G. Li, Y. Yang, Recent progress in polymer solar cells: manipulation of polymer:fullerene morphology and the formation of efficient inverted polymer solar cells, Adv. Mater. 21 (2009) 1434–1449.
[5] J. Peet, Mi.L. Senatore, A.J. Heeger, G.C. Bazan, The role of processing in the fabrication and optimization of plastic solar cells, Adv. Mater. 21 (2009) 1521–1527.
[6] G. Yu, J. Gao, J.C. Hummelen, F. Wudl, A.J. Heeger, Polymer photovoltaic cells: enhanced efficiencies via a network of internal donor–acceptor heterojunctions, Science 270 (1995) 1789–1791.
[7] F.C. Krebs, S.A. Gevorgyan, J. Alstrup, A roll-to-roll process to flexible polymer solar cells: model studies, manufacture and operational stability studies, J. Mat. Chem. 19 (2009) 5442–5451.
[8] F.C. Krebs, T. Tromholt, M. Jørgensen, Upscaling of polymer solar cell fabrication using full roll-to-roll processing, Nanoscale 2 (2010) 873–886.
[9] F.C. Krebs, K. Norrman, Using light-induced thermocleavage in a roll-to-roll process for polymer solar cells, ACS Appl. Mater. Interfaces 2 (2010) 877–887.
[10] F.C. Krebs, S.A. Gevorgyan, B. Gholamkhass, S. Holdcroft, C. Schlenker, M.E. Thompson, B.C. Thompson, D. Olson, D.S. Ginley, S.E. Shaheen, H.N. Alshareef, J.W. Murphy, W.J. Youngblood, N.C. Heston, J.R. Reynolds, S. Jia, D. Laird, S.M. Tuladhar, J.G.A. Dane, P. Atienzar, J. Nelson, J.M. Kroon, M.M. Wienk, R.A.J. Janssen, K. Tvingstedt, F. Zhang, M. Andersson, O. Inganäs, M. Lira-Cantu, R. Bettignies, S. Guillerez, T. Aernouts, D. Cheyns, L. Lutsen, B. Zimmermann, U. Würfel, M. Niggemann, H. Schleiermacher, P. Liska, M. Grätzel, P. Lianos, E.A. Katz, W. Lohwasser, B. Jannon, A round robin study of flexible large-area roll-to-roll processed polymer solar cell modules, Sol. Energy Mater. Sol. Cells 93 (2009) 1968–1977.
[11] F.C. Krebs, T.D. Nielsen, J. Fyenbo, M. Wadstrøm, M.S. Pedersen, Manufacture, integration and demonstration of polymer solar cells in a lamp for the "Lighting Africa" initiative, Energy Environ. Sci. 3 (2010) 512–525.
[12] A.J. Medford, M.R. Lilliedal, M. Jørgensen, D. Aarø, H. Pakalski, J. Fyenbo, F.C. Krebs, Grid-connected polymer solar panels: initial considerations of cost, lifetime, and practicality, Opt. Express 18 (2010) A272–A285.
[13] F. C. Krebs, J. Fyenbo, M. Jørgensen, Product integration of compact roll-to-roll processed polymer solar cell modules: methods and manufacture using flexographic printing, slot-die coating and rotary screen printing, J. Mater. Chem. (2010) ⟨http://dx.doi.org/10.1039/c0jm01178a⟩.
[14] ⟨http://www.solarmer.com/⟩ (accessed on the 1st September 2010).
[15] S.E. Shaheen, C.J. Brabec, N.S. Sariciftci, F. Padinger, T. Fromherz, J.C. Hummelen, 2.5% efficient organic plastic solar cells, Appl. Phys. Lett. 78 (2001) 841–843.
[16] F. Zhang, K.G. Jespersen, C. Björström, M. Svensson, M.R. Andersson, V. Sundström, K. Magunsson, E. Moons, A. Yartsev, O. Inganäs, Influence of solvent mixing on the morphology and performance of solar cells based on polyfluorene copolymer/fullerene blends, Adv. Funct. Mater. 16 (2006) 667–674.
[17] C.N. Hoth, S.A. Choulis, P. Schilinsky, C.J. Brabec, High photovoltaic performance of inkjet printed polymer:fullerene blends, Adv. Mater. 19 (2009) 3971–3978.
[18] F.C. Chen, H.C. Tseng, C.J. Ko, Solvent mixtures for improving device efficiency of polymer photovoltaic devices, Appl. Phys. Lett. 92 (2008) art. no. 103316.
[19] F. Padinger, R.S. Rittberger, N.S. Sariciftci, Effect of postproduction treatment on plastic solar cells, Adv. Funct. Mater. 13 (2003) 85–88.
[20] Y. Kim, S.A. Choulis, J. Nelson, D.D.C. Bradley, S. Cook, J.R. Durrant, Device annealing effect in organic solar cells with blends of regioregular poly(3-hexylthiophene) and soluble fullerene, Appl. Phys. Lett. 86 (2005) 063502.
[21] G. Li, V. Shrotriya, Y. Tao, Y. Yang, Investigation of annealing effects and thin film thickness dependence of polymer solar cells based on poly(3-hexythiophene), J. Appl. Phys. 98 (2005) 043704.
[22] D. Kekuda, J.H. Huang, K.C. Ho, C.W. Chu, Modulation of donor-acceptor interface through thermal treatment for efficient bilayer organic solar cells, J. Phys. Chem. C 114 (2010) 2764–2768.
[23] G. Li, Y. Yao, H. Yang, V. Shrotriya, G. Yang, Y. Yang, "Solvent annealing" effect in polymer solar cells based on poly(3-hexylithiophene) and methanofullerenes, Adv. Funct. Mater. 17 (2007) 1636–1644.
[24] V.D. Mihailetchi, H.X. Xie, B. de Boer, L.M. Popescu, J.C. Hummelen, P.W.M. Blom, L.J.A. Koster, Origin of the enhanced performance in poly(3-hexylithiophene):[6,6]-phenyl C61-butyric acid methyl ester solar cells upon slow drying of the active layer, Appl. Phys. Lett. 89 (2006) 012107.
[25] V. Shrotriya, Y. Yao, G. Li, Y. Yang, Effect of self-organization in polymer/fullerene bulk heterojunctions on solar cell performance, Appl. Phys. Lett. 89 (2006) 063505.
[26] H. Hoppe, N.S. Sariciftci, Morphology of polymer/fullerene bulk heterojunction solar cells, J. Mat. Chem 16 (2005) 45–61.
[27] V. Shrotriya, G. Li, Y. Yao, T. Moriarty, K. Emery, Y. Yang, Accurate measurement and characterization of organic solar cells, Adv. Funct. Mater. 16 (2006) 2016–2023.
[28] D. Chirvase, J. Parisi, J.C. Hummelen, V. Dyakonov, Influence of nanomorphology on the photovoltaic action of polymer-fullerene composites, Nanotechnology 15 (2004) 1317–1323.
[29] J. Huang, Y. Yang, Influence of composition and hear-treatment on the charge transport properties of poly(3-hexylithiophene) and [6,6]-phenyl C_{61}-butyric acid methyl ester blends, Appl. Phys. Lett. 87 (2005) 112105.
[30] A. Swinnen, I. Haeldermans, M. vande Ven, J. D'Haen, G. Vanhoyland, S. Aresu, M. D'Olieslaeger, J. Manca, Tuning the dimensions of C_{60}-based needlelike crystals in blended thin films, Adv. Funct. Mater. 16 (2006) 760–765.
[31] E. Kumacheva, L. Li, M.A. Winnik, D.M. Shinozaki, P.C. Cheng, Direct imaging of surface and bulk structures in solvent cast polymer blend films, Langmuir 13 (1997) 2483–2489.
[32] The video recording the CLSM images continuously for the thin film prepared with 1:1 (P3HT:PCBM) weight ratio can be found in the supplementary material.
[33] M. Dante, J. Peet, T.Q. Nguyen, Nanoscale charge transport and internal structure of bulk heterojunction conjugated polymer/fullerene solar cells by scanning probe microscopy, J. Phys. Chem. C 112 (2008) 7241–7249.